Structure and Properties of Poly(acrylic acid)-Doped Polyaniline

Show-An Chen* and Hsun-Tsing Lee

Department of Chemical Engineering, National Tsing Hua University, Hsinchu 30043, Taiwan, China

Received March 22, 1994; Revised Manuscript Received September 29, 1994®

ABSTRACT: The structure and properties of poly(acrylic acid) (PAA)-doped polyaniline (PAn) (or termed PAA/PAn blend) were investigated by X-ray diffraction, dynamic mechanical analysis, conductivity measurement, ultraviolet–visible–near-infrared spectroscopy, infrared spectroscopy, and atomic force microscopy. The PAA-doped PAn subchains can not align in an ordered fashion as can those of HCl-doped PAn. Therefore, the PAA/PAn blends are amorphous. The blend exhibits a glass transition temperature higher than that of a PAn film plasticized with the same amount of 1-methyl-2-pyrrolidone (NMP), because the doped PAn subchains are more rigid and contain less NMP nearby. During the glass transition, some of the protonated N atoms of PAn are deprotonated due to the increased thermal motion of PAA-doped PAn subchains or, thermodynamically, decreased miscibility between PAA and PAn on heating; the protons generated can combine with the counterions, COO^-, to become COOH. Thus partial undoping of PAn occurs and the conductivity of the blend (2.9×10^{-4} S/cm for the composition of the mole ratio 1/1) drops at temperatures higher than T_g. When the blend is cooled to room temperature, some of the undoped PAn subchains are redoped. For the PAA-doped PAn film, the confinement of carboxylic acid groups on the flexible polymer chains of PAA leads to a nonuniform and inefficient doping, such that some of the acid groups are unable to participate in the the doping and PAA is mainly distributed in the region where PAA-doped PAn subchains aggregate; and the undoped PAn forms another phase, though the acid/base interaction promotes the miscibility between PAA and PAn.

Introduction

Polyaniline (PAn) is an important conducting polymer because of its good environmental stability.[1,2] The conducting form of PAn powder synthesized in aqueous HCl referred to as PAn hydrochloride is insoluble in common organic solvents and even in 1-methyl-2-pyrrolidone (NMP), which is the only organic solvent having been found so far that can dissolve high molecular weight PAn. However PAn base, which can be obtained by treating the PAn hydrochloride with aqueous NH_4OH,[3] is soluble in NMP and can be cast into a flexible film[4–8] with residual NMP as plasticizer.

The dopants usually used for doping PAn are small molecule organic or inorganic acids. These acid dopants can evaporate at room or higher temperature, causing a depression of the conductivity of the acid-doped PAn. This drawback can be overcome by using polymeric acid dopants. In addition, polymeric acid with a glass transition temperature (T_g) lower than that of PAn can be expected to enhance the flexibility of the PAn film.[9] The polymeric acids that have been used as dopants are poly(ethenesulfonic acid),[10] poly(acrylic acid),[10,11] poly(styrenesulfonic acid),[10–14] poly(2-(acrylamido)-2-methyl-1-propanesulfonic acid),[15] and poly(amic acid).[16] These dopants can be incorporated with PAn either during chemical or electrochemical polymerization of aniline or by doping in their aqueous solutions. The polymeric acid dopants can also be used as a template for the oxidative polymerization of aniline, which results in a water soluble PAn.[17,18] However aspects of the microstructures of the polymeric acid-doped PAn including how the dopant interacts with PAn and how the doped PAn subchains align have not been investigated except for poly(amic acid).[16] In addition, due to the confinement of protonic acid groups on polymer chains of the polymeric dopant and to the conformational hindrance created by the flexible chain, it is expected that not all of the acid groups are capable of doping PAn and that nonuniform distribution of the acid groups would occur. Consequently, the microstructure of the polymeric acid-doped PAn and therefore its properties would be different from that of small size protonic acid-doped PAn.

Poly(amic acid)-doped PAn was claimed to be miscible on a molecular scale on the basis of the observation that, after curing by heat treatment, the polyimide in the blend converted from the poly(amic acid) lost its wide angle X-ray scattering (WAXS) deflection peak at $2\theta = 5.9°$.[16] The other nonconjugated polymer, poly(vinylpyrrolidone), which is not a polymeric acid but can form strong hydrogen bonds with the –NH group, has also been blended with PAn. This blend was claimed to be either miscible on the basis of thermal and dynamic mechanical analyses or phase separated with a domain size of 500–1000 Å on the basis of small angle X-ray scattering and optical microscopy.[19]

This work is undertaken to study the microstructure and phase separation in the polymeric protonic acid-doped PAn. Its electronic and optical properties at the temperature range covering the glass transition of the doped PAn are also investigated. Poly(acrylic acid) (PAA) is taken as a model dopant. An understanding of the system should also be applicable to systems with other polymeric protonic acid dopant and would provide valuable information for applications of the doped-PAn in electromagnetic interference shielding, in conductive coatings, and as positive electrodes of electroluminescence diode.[20]

Experimental Section

1. Chemicals. Aniline and hydrochloric acid were synthetic grade from Merck. NMP of synthetic grade was from Ferak Co., Germany. Poly(acrylic acid) (PAA) powder with a weight-average molecular weight of 250 000 was from Aldrich Chemical Co., and its infrared spectrum agrees with that exhibited on page 1346D in *The Aldrich Library of Infrared Spectra*, 2nd ed.

The PAn hydrochloride powder was synthesized by the oxidative polymerization of aniline in 1 M aqueous HCl with

® Abstract published in *Advance ACS Abstracts,* March 1, 1995.

0024-9297/95/2228-2858$09.00/0

$(NH_4)_2S_2O_8$ as oxidant, as described in our previous work,[21] which is similar to the method used by MacDiarmid et al.[22] The powder was converted to PAn base (an emeraldine base) by treatment with 1 M aqueous NH_4OH followed by drying under dynamic vacuum.

The PAn film was prepared by casting a PAn solution in NMP on a Petri dish and drying under dynamic vacuum at 50–60 °C. The resulting film contained a considerable amount of NMP, about 10–18% by weight, due to the high boiling point of NMP (202 °C) and hydrogen-bonding interaction of NMP with PAn.[21,23] The PAA-doped PAn films (or designated as PAA/PAn blends) plasticized with NMP were prepared by mixing appropriate volumes of the two solutions, 0.22 M PAn (based on the approximate repeat unit $-C_6H_4NH-$) in NMP and 0.22 M PAA (based on its repeat unit) in NMP, to give a clear mixed solution, followed by casting the mixed solution on a Petri dish under dynamic vacuum at 50–60 °C. The compositions of the blends are expressed in mole ratios of the repeat units of PAA to those of PAn.

2. Characterization. An X-ray diffractometer (XRD; RigaKu Model D/Max-2B) was used to examine ordering in PAA-doped PAn films. The X-ray beam was nickel-filtered Cu Kα radiation from a sealed tube operated at 30 kV and 20 mA. Data were obtained from 1 to 45° (2θ) at a scan rate of 1°/min.

A thermogravimetric analyzer (TGA; Perkin-Elmer Model TGS-2) was used to measure weight losses of PAA powder, PAn films, and PAA-doped PAn films under a nitrogen stream during a temperature scan from 50 to 600 °C with a heating rate of 10 °C/min.

A dynamic mechanical analyzer (DMA; DuPont Model 983) was used to measure flexural and loss moduli (E' and E'') of cast films of PAA, PAn, and PAA-doped PAn in the temperature range −140 to +250 °C with a heating rate of 2 °C/min and frequency of 1 Hz. The size of the specimens was about 20 mm long, 3 mm wide, and 0.11 mm thick. After a specimen was mounted in the sample chamber, the specimen length subject to cyclic flexural motion was about 1 mm.

Conductivities of the films of PAn and PAA-doped PAn were measured using the four-probe method under dry nitrogen atmosphere from 0 to 175 °C with a heating rate of 2 °C/min.

An ultraviolet–visible–near-infrared recording spectrophotometer (UV–vis–near-IR; Perkin-Elmer Lambda 19) was used to measure optical absorbances in the wavelength range 200–2500 nm of solid films coated on glass plates.

An infrared spectrophotometer (IR; Perkin-Elmer Model 983) was used to identify the chemical structures of PAA, PAn, PAA-doped PAn, and NMP. Solid specimens of PAA, PAn, and PAA-doped PAn were prepared by grinding powdery samples with KBr powder and then pressing the mixtures into tablets. NMP was examined as a thin liquid film on a KBr crystal surface.

A scanning electron microscope (SEM; Hitachi Model S-570) was used to examine morphologies of films of PAn and PAA-doped PAn. A piece of film of about 1 mm × 2 mm in size was fixed on the sample holder using adhesive tape and was then coated with a thin layer of gold to improve image resolution.

Atomic force microscopy (AFM) scans were performed using a Nanoscope III instrument from Digital Instruments. For the AFM technique, a very sharp probe on a flexible cantilever contacts the sample surface to sense the topography of the sample, and an optical head is used to sense the cantilever deflection by sensing the change in position of a laser beam which is reflected off the back of the cantilever. The solution of 0.22 M PAn in NMP was coated on a highly ordered pyrolytic graphite substrate by spin-casting and then drying by evaporation of NMP at room temperature, followed by further drying at 50–60 °C under dynamic vacuum. HCl-doped PAn was prepared by immersing the PAn film coated on a piece of graphite in 1 M aqueous HCl. The so obtained films on graphite surfaces were scanned by AFM. PAA-doped PAn films on graphite for AFM scanning with the mole ratios of their repeat units PAA/PAn as 1/1, 1/2, and 1/4 were prepared similarly to the PAn film on graphite. An NMP (16 wt %)-plasticized PAn free-standing film after extraction with tetrahydrofuran for 18 days was also scanned by AFM.

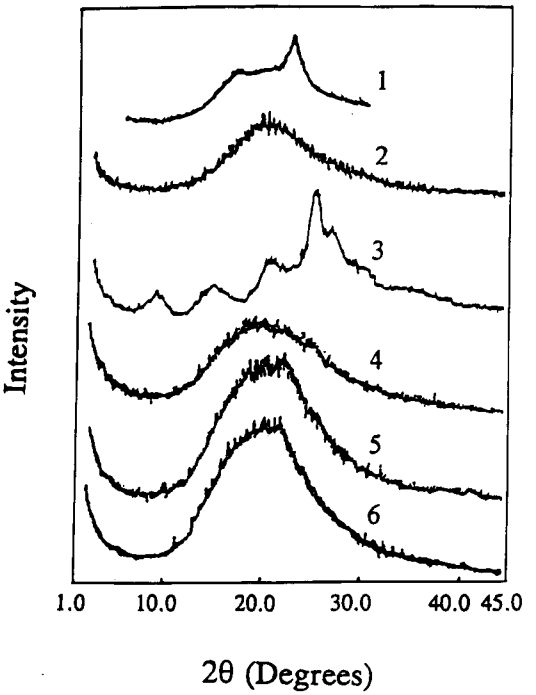

Figure 1. X-ray diffraction pattners of the (1) PAA film, (2) PAn film, (3) HCl-doped PAn powder, (4) PAA/PAn (1/1) blend, (5) PAA/PAn (1/2) blend, and (6) PAA/PAn (1/4) blend.

Results and Discussion

X-ray Diffraction (XRD) Patterns. XRD patterns of PAA, the PAn film, the HCl-doped PAn powder, and PAA-doped PAn films with compositions of PAA/PAn of 1/1, 1/2, and 1/4 are shown in Figure 1. The PAn film exhibits a broad amorphous reflection at $2\theta = 19°$, while the HCl-doped PAn powder has several diffraction peaks, indicating that PAn subchains become more rigid and ordered after the doping. On the contrary, there are no pronounced diffraction peaks in the patterns of PAA/PAn blends, indicating that PAA-doped PAn subchains are much more randomly aligned. This results from the conformational hindrance and large size of the PAA chains, which makes an ordered packing of the PAn subchains difficult. The PAA film exhibits a reflection peak at 22° and a shoulder at 17°. However the reflection peak at 22° cannot be identified in the XRD spectra of the blends, indicating a strong interaction between these two polymers.

Thermogravimetric Analysis (TGA). Figure 2 shows the results of TGA measurements of the PAA powder, PAn film, and PAA-doped PAn film with the 1/1 composition of PAA/PAn. The PAn film and PAA/PAn (1/1) blend are both plasticized with 15 wt % NMP, while the PAA powder contains no NMP. When these samples were heated at 110 °C for 10 min prior to TGA measurement, the weights of these samples remain unchanged before 120 °C.[21] The weight losses (about 1.5 wt %) before 110 °C of these samples are due to losses of adsorbed moisture. The water contents of the pure PAA powder are 2–3 wt %, and the majority of water can be removed by heating to 90 °C. For the PAn film plasticized with 15 wt % NMP, the weight losses due to evaporation of NMP start at about 120–130 °C and end at about 420–480 °C, above which the weight losses are due to the decomposition of PAn.[21] By use of the TGA measurement, the NMP content of the PAn

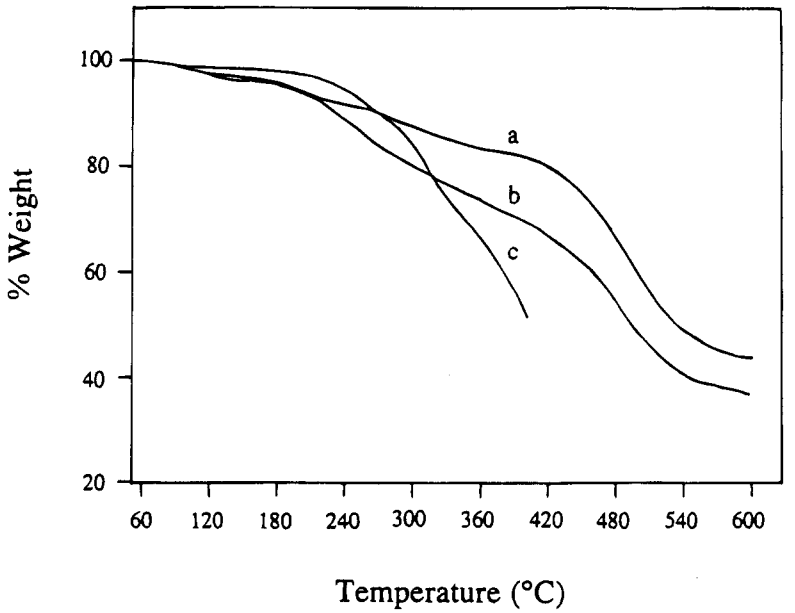

Figure 2. TGA curves of the (a) PAn film (contains 15 wt % NMP), (b) PAA/PAn (1/1) blend (contains 15 wt % NMP), and (c) PAA powder.

film was determined by counting the total weight losses as the temperature rises to 420 °C. For the PAA/PAn (1/1) blend, the NMP content is 15 wt %, as determined by elemental analysis. For the blend, TGA cannot be used to determine the NMP content, since the weight losses in the range 180–480 °C are due to both evaporation of NMP and decomposition of PAA.

Dynamic Mechanical Analysis (DMA). DMA results (flexural modulus E' and loss modulus E'') of films of PAA, PAn, and PAA/PAn blends with the compositions 1/1, 1/2, and 1/4 are shown in Figure 3. These films are all plasticized with 15 ± 1 wt % NMP. The NMP contents of the PAA film and PAA/PAn blends are determined by the elemental analysis and that of the PAn film is by TGA. The E'' curve of the PAA film plasticized with NMP has two peaks centered at about −65 and +68 °C. The peak at 68 °C is the glass transition temperature (T_g) of this NMP-plasticized PAA film, because its E' drops by 2 orders during the transition. From E'' curves of the PAn film and PAA/PAn blends, three transitions (β, α, and α') are observed, and their characteristic temperatures are listed in Table 1. The second transition temperature (T_α) can be assigned as the glass transition temperature, because E' drops by 1–2 orders in this transition region. The glass transition temperature of PAn is consistent with the result obtained by Wei.[5,24] As the temperature increases beyond this transition region, E' changes from a rapid decrease to a rapid increase until a maximum is reached and then to a rapid decrease again; E'' also exhibits similar changes and generates a new peak after the α transition, which is designated as the α' transition. This α' transition results from a competition between the two factors: (a) increase in stiffness due to further evaporation of NMP and an occurrence of cross-linking reaction[21] and (b) decrease in stiffness due to increased segmental thermal motion caused by the raising temperature. While in the β transition region at the low-temperature range, E' drops by less than 0.1 order and E'' exhibits a transition centered at −80 to −65 °C. Since PAn has no side chain, this transition can be attributed to the moisture absorbed in these films, as in the case of poly(caprolactam).[25]

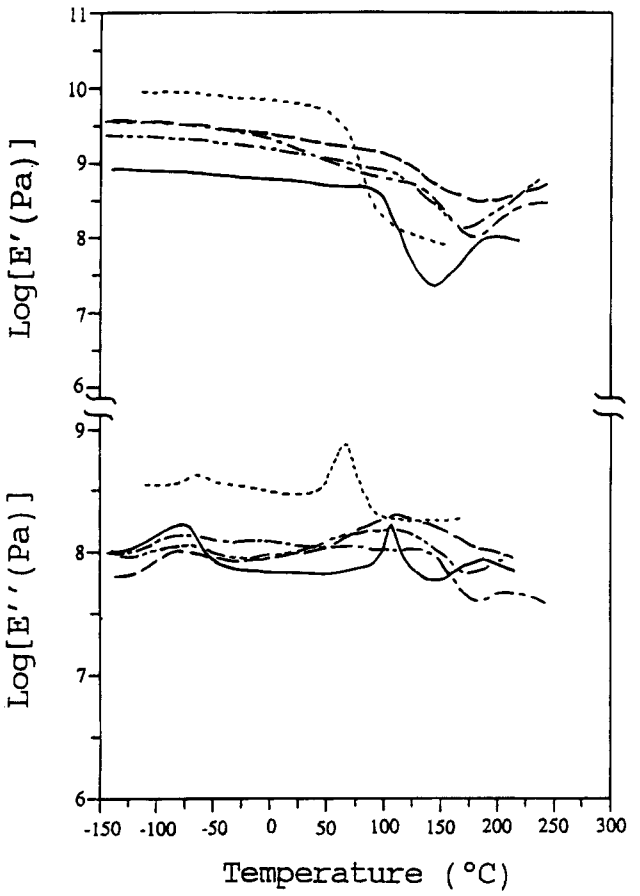

Figure 3. Dynamic mechanical analysis of various NMP plasticized films at the frequency 1 Hz and heating rate 2 °C/min: (- - -) PAA film; (—) PAn film; (— · —) PAA/PAn (1/1) blend; (— · · —) PAA/PAn (1/2) blend; (— — —) PAA/PAn (1/4) blend.

T_α's of the PAA/PAn blends with the compositions 1/4, 1/2, and 1/1 are 109, 112, and 125 °C, respectively (Table 1). The T_α increases with the PAA content (or the doping level) and is higher than that of the PAn plasticized with 15 wt % NMP (105 °C) by 4–20 °C. The α transitions also complete at temperatures (170–180 °C) higher than that of the PAn plasticized with 15 wt

Table 1. Transition Temperatures (°C) of PAn, PAA, and PAA/PAn Blends from Dynamic Mechanical Analysis

	transition temp (°C)						
	β			α			α′
sample[a]	onset	max	end	onset	max	end	max
PAA	−95	−65	−25	35	68	105	none
PAn	−130	−78	−20	65	105	130	190
PAA/PAn (1/4)	−130	−80	−19	30	109	175	pr[b]
PAA/PAn (1/2)	−122	−75	−25	20	112	170	202
PAA/PAn (1/1)	−135	−75	−25	100	125	180	206

[a] All contain about 15 wt % NMP; PAA is poly(acrylic acid); the number in the parentheses is the mole ratio of the repeat units of PAA to PAn. [b] Poor resolution.

% NMP (130 °C). The increase of T_α is due to the more rigid PAn subchains after doping and the lower NMP content in the vicinity of PAA-doped PAn subchains (because PAA-doped PAn subchains are insoluble in NMP, most of the NMP will be expelled away from the vicinity of these subchains during the film formation process). Since PAA has no α′ transition and its weight losses are less than 3 wt % during the heating scan at temperatures below 210 °C (Figure 2), the occurrence of the α′ transition of the PAA/PAn blend is attributed to the PAn-rich phase in which the PAA content is much less than that of the PAA-doped PAn phase. $T_{\alpha'}$ of the PAA/PAn blend is higher than that of PAn (190 °C) by 12−16 °C due to the same reason, that its T_α is higher than that of the PAn, as stated above.

The temperature range of α (or β) transitions of PAA/PAn blends covers that of α (or β) transitions of PAn and PAA, so that it is difficult to evaluate the compatibility between PAn and PAA by DMA. But there are two transition regions in the E' curve of the PAA/PAn (1/1) blend, one in the range 25−75 °C and the other in the range 100−150 °C. The T_g of PAA (68 °C) falls in the former region, and that of PAn (105 °C) and the PAA/PAn (1/1) blend (125 °C), in the latter region. Thus, in the PAA/PAn blends, phase separation is likely to occur.

Conductivity Measurement. The conductivities of films of the PAn film and PAA/PAn blends with the compositions 1/4, 1/2, and 1/1 at various temperatures are shown in Figure 4. In the temperature range 0−175 °C, each film has a conductivity maximum. The peak conductivity and its corresponding temperature are listed in Table 2. Each conductivity curve of these three blends exhibits a shoulder within 50−110 °C, but not for PAn. This shoulder can be attributed to the presence of a considerable amount of moisture in the blend due to the hygroscopic nature of PAA, as to be elucidated below. Let the PAA/PAn (1/1) blend be subjected to conductivity measurement six times over different temperature ranges under a dry nitrogen stream. This blend was first measured in the range 30−50 °C. After cooling to 30 °C, it was then measured in the range 30−80 °C. The above heating scan was repeated four times more, but the upper temperature limit was increased successively. For the last scan, the temperature range is 30−160 °C. The results are shown in Figure 5. The shoulder in the conductivity curve of this blend becomes more and more vague as the number of scans increases and finally disappears in the sixth scan (30−160 °C). Since the moisture (about 1.5 wt %) evaporates after the heating scan to 110 °C, the shoulder in Figure 4 thus results from the moisture absorbed by PAA.

For the PAn film, the temperature at the conductivity maximum (130 °C, Table 2) is 25 °C higher than T_α (105 °C, Table 1). The presence of a conductivity maximum can be attributed to the occurrence of α relaxation of PAn subchains, as illustrated below. Although the electron mobility increases with increasing temperature, it is compensated for by the increased ring distortion in the PAn subchains due to the α relaxation. These

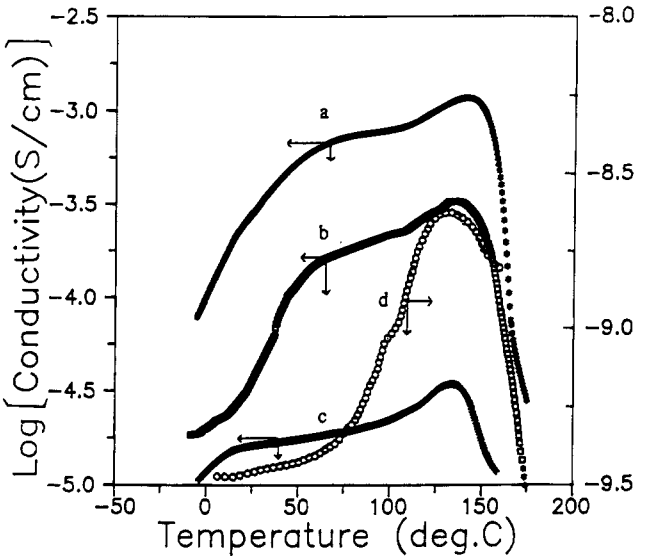

Figure 4. Conductivity versus temperature curves of the (a) PAA/PAn (1/1) blend, (b) PAA/PAn (1/2) blend, (c) PAA/PAn (1/4) blend, and (d) PAn film.

Table 2. Conductivity Maxima and Transition Temperatures of PAn and PAA/PAn Blends from the Heating Scan of Conductivity Measurement[a]

sample[b]	T_{max}[c] (°C)	σ_{max}[d] (S/cm)	$\sigma_{25,i}$[e] (S/cm)	$\sigma_{25,k}$[f] (S,cm)
PAn	130	2.4×10^{-9}	10^{-10}−10^{-9}	
PAA/PAn (1/4)	133	3.4×10^{-5}	1.6×10^{-5}	4.5×10^{-6}
PAA/PAn (1/2)	135	3.3×10^{-4}	3.5×10^{-5}	6.6×10^{-6}
PAA/PAn (1/1)	140	1.2×10^{-3}	2.9×10^{-4}	1.0×10^{-5}

[a] Using the four-point method. [b] All contain about 15 wt % NMP. [c] The temperature at which the conductivity reaches a maximum. [d] The maximum conductivity. [e] The conductivity at 25 °C before the heating scan. [f] The conductivity at 25 °C after the heating scan to 175 °C.

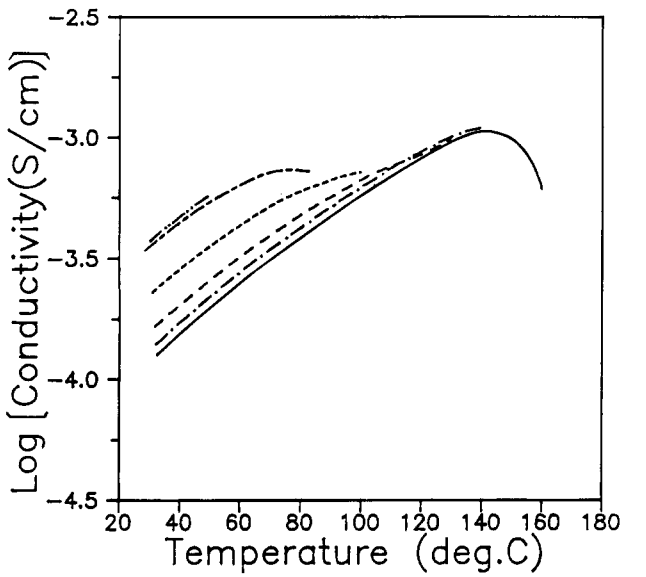

Figure 5. Conductivity versus temperature curves of the PAA/PAn (1/1) blend during six successive heating scans: (−··−) first; (− - −) second; (- - -) third; (− − −) fourth; (−·−) fifth, (—) sixth.

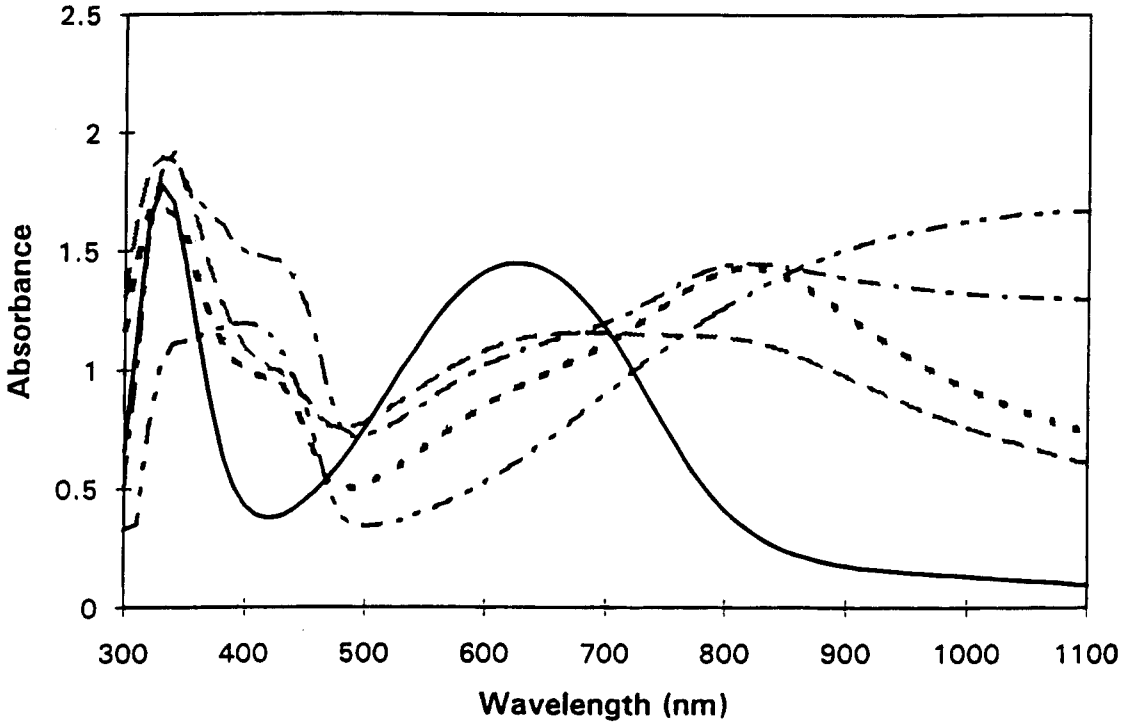

Figure 6. UV–vis spectra of doped PAn films: (—) PAn film, (– ··) HCl-doped PAn film; (– · –) PAA/PAn (1/1) blend; (- - -) PAA/PAn (1/2) blend; (– –) PAA/PAn (1/4) blend.

two factors compete during the relaxation period. As temperature increases, the latter becomes more important than the former; the conductivity then drops. Thus the temperature at the conductivity maximum can be expected to be higher than T_α, as is just the case. After the completion of the α relaxation process, a further increase of temperature leads to a more pronounced motion of subchains. Thus the conductivity decreases with a further increase of temperature. Such a phenomenon also occurs in poly(3-alkylthiophene)s with the carbon number of the alkyl side chain at or higher than 4, as reported by one of us.[26,27]

For the PAA/PAn blends with compositions 1/4, 1/2, and 1/1, the temperatures at the conductivity maxima are 133, 135, and 140 °C, respectively. The T_α are 109, 112, and 125 °C, respectively, for the above three blends. For each PAA/PAn blend, the temperature at the conductivity maximum (Table 2) is 15–24 °C higher than T_α. The T_α and temperature at the conductivity maximum both increase with PAA content. The presence of conductivity maxima of the blends can be attributed to the occurrence of α relaxation of PAA-doped PAn subchains or, thermodynamically, the increase of phase separation between PAA and PAn on heating.[28] During α relaxation, thermal motion of PAA-doped PAn subchains causes parts of the protons originally bonded with the N atoms to become debonded and subsequently to couple with the counterions COO^- to become COOH. This partial undoping of the PAn gives a drop in conductivity which is similar to that of the HCl-doped PAn reported in the literature.[29–31] This thermal undoping phenomenon can also be observed from the UV–vis–near-IR spectroscopical examination in the next section. The conductivities of the blends measured at room temperature were lowered by about 1 order after the heating scan to 160–175 °C (Table 2). The conductivities of the blends cannot be recovered completely after the heat treatment.

Ultraviolet–Visible–Near-Infrared (UV–vis–near-IR) Spectroscopy. The UV–vis spectra of films of PAn, HCl-doped PAn, and PAA/PAn blends with the compositions 1/1, 1/2, and 1/4 are shown in Figure 6. The UV–vis spectrum of the PAn has two absorption peaks at 324 and 639 nm, which are due to the $\pi-\pi^*$ transition of the benzenoid rings and the exciton absorption of the quinoid rings, respectively.[32,33] In the PAn, half of the N atoms are in amine groups and the other half are in imine groups. Since only the imine groups can be doped by acid, the maximum doping level of the PAn is 0.5. While the N atoms in the imine groups are protonated, N and its neighboring quinoid ring become a semiquinoid radical cation[34] and the exciton absorption peak intensity decreases. When the N atoms in the imine groups are fully protonated, as the doping level is 0.5, the exciton absorption peak of PAn would disappear, as in the case of HCl-doped PAn in Figure 6. If every carboxylic acid group is able to dope PAn, the PAn would be fully doped in the PAA/PAn (1/2) blend, and the acid groups would be in excess in the PAA/PAn (1/1) blend. However, the exciton absorption peak appears in all these blends and the doping level seems to increase with increasing PAA content, as reflected in the increase of absorption in the range 700–1100 nm. This implies that there are undoped PAn in these blends and that phase separation exists, which can be attributed to conformational hindrance of the long chain PAA (M_w = 250 000), which prevents parts of the carboxylic acid groups from a protonation of the imine N atoms. The weak acid –COOH is not a factor for the ineffective doping of PAA, because the UV–vis spectrum and conductivity of acetic acid-doped PAn are nearly the same as those of HCl-doped PAn.[4,35]

The PAA/PAn (1/1) blend with film thickness 0.2–0.4 μm was subject to a heating scan from 25 to 80 °C under a nitrogen stream and then purging with saturated water vapor at 25 °C for 2 h. The UV–vis–near-IR spectrum at each stage of the above thermal treatment is shown in Figure 7a. The blend was further subjected to a second heating scan from 25 to 150 °C

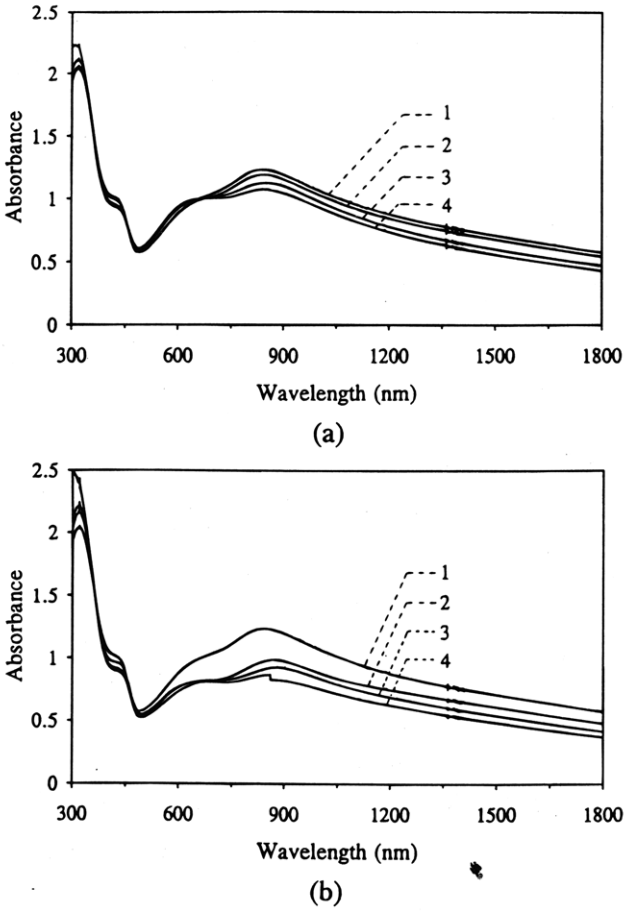

Figure 7. UV–vis-near-IR spectra of the PAA/PAn (1/1) blend: (a) (1) at 25 °C before the heating scan, (2) at 25 °C after the heating scan to 80 °C and purging with saturated water vapor for 2 h, (3) at 25 °C after the heating scan to 80 °C, (4) at 80 °C; (b) (1) at 25 °C before the heating scan, (2) at 25 °C either after the heating scan to 150 °C and purging with saturated water vapor for 2 h or after the heating scan to 150 °C annealing at 70 °C under nitrogen stream or saturated water vapor for 1.5 h and purging with saturated water vapor for 2 h, (3) at 25 °C after the heating scan to 150 °C, (4) at 150 °C.

under a nitrogen stream, then annealing at 70 °C under a nitrogen stream or under saturated water vapor for 1.5 h, and finally purging with saturated water vapor at 25 °C for 2 h. The UV–vis–near-IR spectrum at each stage of this thermal treatment is shown in Figure 7b. These spectra show that the π–π^* absorption of PAn increases and the absorption of PAn in the range 700–1800 nm decreases when the blend was heated to 80 °C and to 150 °C. This indicates that partial thermal undoping of the blend occurs. When the heated blend was cooled to 25 °C, the π–π^* absorption of PAn decreases and the absorptions of PAn in the range 700–1800 nm increase slightly, indicating that partial redoping of PAn occurs. The blend after the heating was further purged with saturated water vapor at 25 °C for 2 h to see if the incomplete recovery of the doping level of PAn is due to a loss of adsorbed moisture. After the blend absorbed moisture, the counteranion was solvated, resulting in a reduced pinning of the polaron on the PAn subchain in the vicinity of the anion and a greater delocalization of the polaron on the PAn subchain.[36] Thus, the absorption in the 700–1800 nm region increases, as indicated in curve 2 in both Figure 7a,b. However the blend still cannot completely recover from its original doping level after the absorption of moisture. Thus, some of the protonated N atoms of PAn

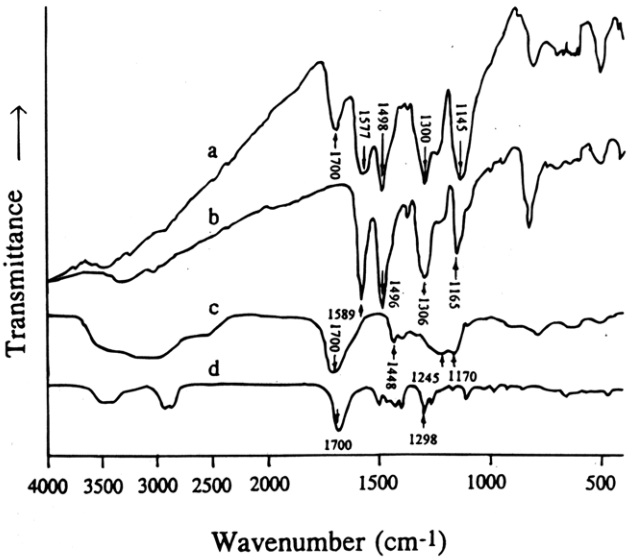

Figure 8. IR spectra of the (a) the PAA/PAn (1/1) blend, (b) PAn, (c) PAA, and (d) NMP.

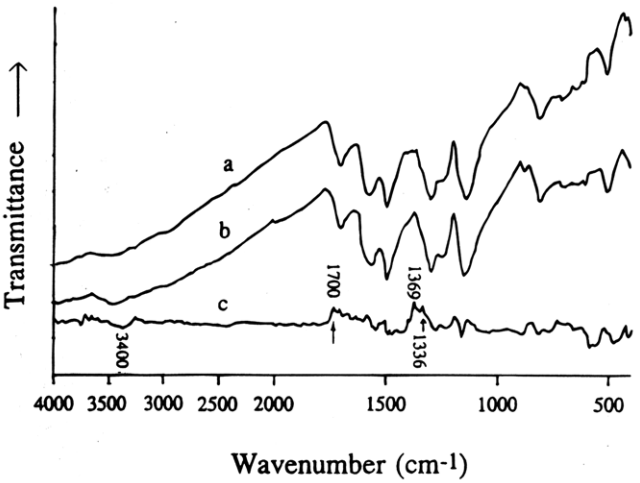

Figure 9. IR spectra of the PAA/PAn (1/1) blend measured at 25 °C: (a) before the heating scan; (b) after the heating scan to 150 °C; (c) the spectrum obtained by subtracting (a) from (b).

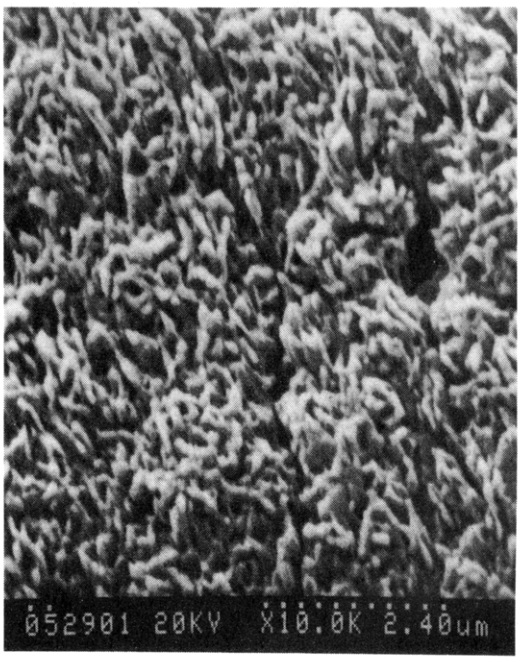

Figure 10. SEM micrograph of THF-extracted NMP-plasticized PAn film.

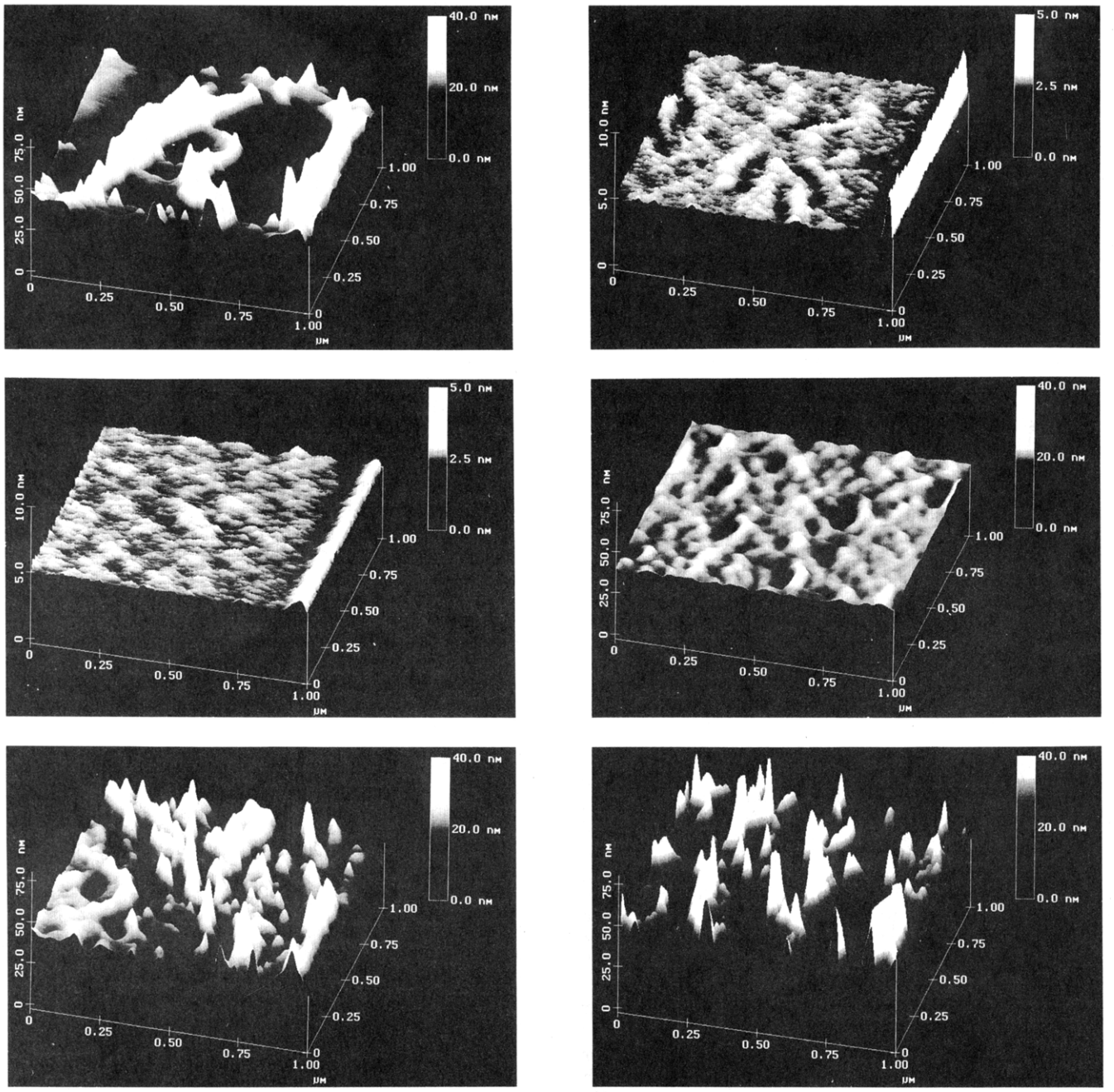

Figure 11. AFM images of (a, top left) a THF-extracted free-standing PAn film, (b, top right) a PAn film on a highly ordered, pyrolytic graphite surface, (c, middle left) a HCl-doped PAn film on a highly ordered, pyrolytic graphite surface, (d, middle right) the PAA/PAn (1/1) blend on a highly ordered, pyrolytic graphite surface, (e, bottom left) the PAA/PAn (1/2) blend on a highly ordered, pyrolytic graphite surface, and (f, bottom right), the PAA/PAn (1/4) blend on a highly ordered pyrolytic graphite surface.

are deprotonated due to thermal motion of PAA-doped PAn subchains or due to lower miscibility between PAA and PAn at 80 °C or above and are partially redoped as the thermal motion of PAn subchains reduces when the blend cools to room temperature. The blend fails to completely recover its doping level even when it is annealed at 70 °C (slightly above the T_g of NMP (15 wt %)-plasticized PAA, 68 °C) under a nitrogen stream or saturated water vapor for 1.5 h and then purged with saturated water vapor at 25 °C for 2 h, as indicated by curve 2 in Figure 7b.

Infrared Spectroscopy (IR). The IR spectra of PAA, the PAn powder, NMP, and the PAA/PAn (1/1) blend (which is plasticized with 15 wt % NMP) are shown in Figure 8. The main characteristic absorptions are as follows: for NMP, 1700 cm^{-1} (C=O stretching) and 1298 cm^{-1} (C—N stretching); for PAA, 2900–3600 cm^{-1} (—OH stretching), 1700 cm^{-1} (C=O stretching), 1448 cm^{-1} ($-CH_2-$ scissor vibration), and 1245 and 1170 cm^{-1} (both due to C—O stretching); for PAn, 1589 cm^{-1} (C=C stretching of the quinoid rings),[21] 1496 cm^{-1} (C=C stretching of the benzenoid rings),[21] 1306 cm^{-1} (C—N stretching), and 1165 cm^{-1} (electronic-like absorption of N=Q=N[37] where Q denotes the quinoid ring); for the blend, broad absorption in 2000–4000 cm^{-1} (free carriers absorption)[38] and 1145 cm^{-1} (the electronic-like absorption)[37] both due to the doping of PAn.

The IR spectra of the PAA/PAn (1/1) blend at room temperature before (spectrum a) and after heating to 150 °C (spectrum b) are shown in Figure 9. Spectrum c is obtained by subtracting spectrum a from spectrum b, in which the absorption peaks above the baseline indicate a decrease of the amounts of their correspond-

ing functional groups, while those below indicate an increase. The decrease in the absorption peak at 1700 cm^{-1} due to C=O stretching indicates a loss of NMP. The decrease in the absorption peaks at 1369 and 1336 cm^{-1} (due to symmetric stretching of COO^-) and the increase of the broad absorption peak around 3400 cm^{-1} (due to −OH stretching) reflect a decrease in COO^- and an increase in COOH, resulting from an occurrence of undoping. This observation is in agreement with those from conductivity and UV−vis−near-IR measurements.

Atomice Force Microscopy (AFM). All the scanning electron microscopy (SEM) images of films of PAn, HCl-doped PAn, and PAA-doped PAn with the ratios of PAA/PAn of 1/1, 1/2, and 1/4 exhibit smooth and featureless surface morphology; thus SEM cannot be used to distinguish the morphology differences among these films. In order to study the morphologies of these films and to investigate the compatibility between PAA and PAn, AFM was used. The AFM images of the NMP-plasticized PAn free-standing film after extraction with tetrahydrofuran (THF) for 18 days, the PAn film, the HCl-doped PAn film, and PAA-doped PAn films with the ratios of PAA/PAn of 1/1, 1/2, and 1/4 are shown in Figure 11. The NMP-plasticized PAn free-standing film after extraction with THF for 18 days was first subjected to examination by AFM and SEM. The AFM image of the film shows a fibrilar morphology with a fiber diameter about 0.1 μm (Figure 11a), similar to that observed by SEM (Figure 10). However, it appears that AFM has a much high resolution than SEM and provides more detailed information about the surface morphology of the film. The morphological examination of HCl and PAA-doped PAn films is described below.

The surface morphology with height ruggedness scale 5 nm of the PAn film cast on a highly ordered, pyrolytic graphite surface looks like aggregates of small globules (Figure 11b). After the PAn film was doped in 1 M aqueous HCl to give a surface conductivity of 10 S/cm (by the four-probe method), its surface morphology (Figure 11c) is the same as that before the HCl doping. For the PAA-doped PAn film with the PAA/PAn ratio 1/1, the AFM image (Figure 11d) shows a fibrilar network morphology with height ruggedness scale 40 nm, which is larger than that (5 nm) used by the image of the HCl-doped PAn film. The protruded regions of the fibrilar network are composed of the aggregates of PAA-doped PAn subchains for the following reasons: (1) more rigid PAA-doped PAn subchains, (2) the presence of interaction between neighboring PAA-doped PAn subchains, and (3) PAA-doped PAn being insoluble in NMP, so that NMP will be expelled out from the region where PAA-doped PAn subchains aggregated. The presence of connected protruded regions leads to a conductivity of this film as high as 3×10^{-4} S/cm. As the PAA content is reduced, the amount of the protruded region decreases accordingly, as can be seen in Figure 11e,f for PAA-doped PAn films with the PAA/PAn ratios of 1/2 and 1/4, respectively. In these two films, the PAA content is insufficient to form a network morphology; a partly protruded wedge-like morphology is observed.

From the AFM study above, it is clear that the loss of the XRD characteristic peak of PAA in the blend does not ensure miscibility in our case. The morphology of the polymeric acid-doped PAn is quite different from that of the small size acid-doped PAn. This is due to the fact that the carboxylic acid groups of PAA are confined on the polymer chains and cannot diffuse casually, so they are not all effective for doping PAn. Such confinement also leads to a phase separation and loss of ordered alignment of PAn subchains in the bulk of the films. The domain size of the phase of PAA-doped PAn and PAA is about 0.05 μm.

Conclusion

For the PAA-doped PAn (or termed PAA/PAn blend), the confinement of carboxylic acid groups on the flexible polymer chain of PAA leads to a nonuniform and inefficient doping, such that some of the acid groups are not able to participate in the doping and PAA is mainly distributed in the region where PAA-doped PAn subchains aggregate. Thus phase separation occurs in the blend, and the doped PAn subchains are difficult to align in an ordered fashion, unlike the HCl-doped PAn. The blend exhibits a glass transition temperature higher than that of the PAn film plasticized with the same amount of NMP, because the doped PAn subchains are more rigid and contain less NMP nearby. During the glass transition, PAA-doped PAn subchains become more flexible and some of the protonated N atoms of PAn are deprotonated due to the increased thermal motion or decreased miscibility on heating; the protons generated can combine with the counterions, COO^-, to become COOH. Thus partial undoping of PAn occurs and the conductivities of the blends drop at temperatures higher than T_g. When the blend is cooled to room temperature, some of the thermally undoped PAn subchains are redoped.

Acknowledgment. We wish to thank the National Science Council of the ROC for financial aid through the project NSC 82-0416-E007-156.

References and Notes

(1) Chen, S. A.; Fang, W. G. *Macromolecules* **1991**, *24*, 1242.
(2) Genies, E. M.; Lapkowski, M. *Synth. Met.* **1988**, *24*, 61.
(3) Chiang, J. C.; MacDiarmid, A. G. *Synth. Met.* **1986**, *13*, 193.
(4) Angelopoulos, M.; Ray, A.; MacDiarmid, A. G.; Epstein, A. J. *Synth. Met.* **1987**, *21*, 21.
(5) Wei, Y.; Jang, G. W.; Hsueh, K. F.; Scherr, E. M.; MacDiarmid, A. G.; Epstein, A. J. *J. Polym. Mater. Sci. Eng.* **1989**, *61*, 916.
(6) MacDiarmid, A. G.; Epstein, A. J. *Faraday Discuss. Chem. Soc.* **1989**, *88*, 317.
(7) Monkman, A. P.; Adams, P. *Synth. Met.* **1991**, *40*, 87.
(8) Cromack, K. R.; Jozefowicz, M. E.; Ginder, J. M.; Epstein, A. J.; McCall, R. P.; Du, G.; Leng, J. M.; Kim, K.; Li, C.; Wang, Z. H.; Druy, M. A.; Glatkowski, P. J.; Scherr, E. M.; MacDiarmid, A. G. *Macromolecules* **1991**, *24*, 4157.
(9) Rubner, M. F.; Tripathy, S. K.; Georger, J.; Cholewa, P. *Macromolecules* **1983**, *16*, 870.
(10) Hwang, J. H.; Yang, S. C. *Synth. Met.* **1989**, *29*, E271.
(11) Liu, J. M.; Yang, S. C. *J. Chem. Soc., Chem. Commun.* **1991**, 1529.
(12) Li, S.; Dong, H.; Cao, Y. *Synth. Met.* **1989**, *29*, E329.
(13) Malhotra, B. D.; Ghosh, S.; Chandra, R. *J. Appl. Polym. Sci.* **1990**, *40*, 1049.
(14) Kang, Y.; Lee, M. H.; Rhee, S. B. *Synth. Met.* **1992**, *52*, 319.
(15) Lapkowski, M. *Synth. Met.* **1993**, *55−57*, 1558.
(16) Angelopoulos, M.; Patel, N.; Saraf, R. *Synth. Met.* **1993**, *55−57*, 1552.
(17) Angelopoulos, M.; Patel, N.; Shaw, J. M. *Mater. Res. Soc. Symp. Proc.* **1994**, *328*, 173.
(18) Angelopoulos, M.; Patel, N.; Shaw, J. M.; Labianca, N. C.; Rishton, S. A. *J. Vac. Sci. Technol. B* **1993**, *11*, 2794.
(19) Stockton, W. B.; Rubner, M. F. *Mater. Res. Soc. Symp. Proc.* **1994**, *328*, 257.
(20) Gustafsson, G.; Cao, Y.; Treacy, G. M.; Klavetter, F.; Colaneri, N.; Heeger, A. J. *Nature* **1992**, *357*, 477.
(21) Chen, S. A.; Lee, H. T. *Macromolecules* **1993**, *26*, 3254.
(22) Asturias, G. E.; MacDiarmid, A. G.; McCall, R. P.; Epstein, A. J. *Synth. Met.* **1989**, *29*, E157.
(23) Chen, S. A.; Lee, H. T. *Synth. Met.* **1992**, *47*, 233.

(24) Wei, Y.; Jang, G. W.; Hsueh, K. F.; Scherr, E. M.; MacDiarmid, A. G.; Epstein, A. J. *Polymer* **1992**, *33*, 314.
(25) (a) Nielsen, L. E. *Mechanical Properties of Polymers and Composites*; Marcel Dekker Inc.: New York, 1974; p 195. (b) Kolarik, J.; Janacek, J. *J. Polym. Sci.* **1967**, *C16*, 441.
(26) Chen, S. A.; Ni, J. M. *Makromol. Chem., Rapid Commun.* **1991**, *13*, 31.
(27) Chen, S. A.; Ni, J. M. *Macromolecules* **1992**, *25*, 6081.
(28) Olabisi, O.; Robeson, L. M.; Shaw, M. T. *Polymer-Polymer Miscibility*; Academic Press: New York, 1979; p 91.
(29) Wei, Y.; Hsueh, K. F. *J. Polym. Sci., Polym. Chem.* **1989**, *27*, 4351.
(30) Kulkarni, V. G.; Campbell, L. D.; Mathew, W. R. *Synth. Met.* **1989**, *30*, 321.
(31) Yue, J.; Epstein, A. J.; Zhong, Z.; Gallagher, P. K.; MacDiarmid, A. G. *Synth. Met.* **1991**, *41–43*, 765.
(32) Lu, F. L.; Wudl, F.; Nowak, M.; Heeger, A. J. *J. Am. Chem. Soc.* **1986**, *108*, 8311.
(33) Stafstrom, S.; Bredas, J. L.; Epstein, A. J.; Woo, H. S.; Tanner, D. B.; Huang, W. S.; MacDiarmid, A. G. *Phys. Rev. Lett.* **1987**, *59*, 1464.
(34) Furukawa, Y.; Ueda, F.; Hyodo, Y.; Harada, I.; Nakajima, T.; Kawagoe, T. *Macromolecules* **1988**, *21*, 1297.
(35) Zuo, F.; McCall, R. P.; Ginder, J. M.; Roe, M. G.; Leng, J. M.; Epstein, A. J.; Asturias, G. E.; Ermer, S. P.; Ray, A.; MacDiarmid, A. G. *Synth. Met.* **1989**, *29*, E445.
(36) Chiang, J. C.; MacDiarmid, A. G. *Synth. Met.* **1986**, *13*, 193.
(37) Salaneck, W. R.; Liedberg, B.; Inganas, O.; Erlandsson, R.; Lundstrom, I.; MacDiarmid, A. G.; Halpern, M.; Somasiri, N. L. D. *Mol. Cryst. Liq. Cryst.* **1985**, *121*, 191.
(38) Tourillon, G. In *Handbook of Conducting Polymers*; Skotheim, T. A., Ed.; Marcel Dekker Inc.: New York and Basel, 1986; p 319.

MA9412243